ACCSCIENCE PUBLISHING

Materials Science in Additive Manufacturing

ORIGINAL RESEARCH ARTICLE

Reactive selective laser melting of silicon carbide

Tsovinar Ghaltaghchyan[1]*, Khachik Nazaretyan[2], Ani Khachikyan[1], and Marina Aghayan[1]

[1]3D printing Research Laboratory, A.B. Nalbandyan Institute of Chemical Physics NAS RA, Yerevan, Armenia

[2]Laboratory of Macrokinetics of Solid-State Reactions, A.B. Nalbandyan Institute of Chemical Physics NAS RA, Yerevan, Armenia

Abstract

Additive manufacturing of silicon carbide (SiC) is challenging due to uncontrollable quality, surface roughness of fabricated parts, expensive post-processing, and long production times for customized components. Developing cost-effective, rapid manufacturing techniques that maintain high quality and design freedom is therefore highly desirable. In this study, laser powder bed fusion (LPBF) followed by ultra-fast post heat treatment was applied to produce SiC-based composites using silicon and carbon powders as raw materials. The influence of processing parameters on silicon-carbon reaction and sintering was investigated. Boron carbide was used as an additive to enhance sintering. Substantial SiC formation occurred despite the limited heating time. Boron carbide influenced both SiC formation and grain growth. The maximum Vickers hardness (1218 $HV_{0.2}$) was achieved in boron carbide-containing heat-treated samples printed at a laser power of 48 W. This novel approach enables the efficient fabrication of SiC-based composites with enhanced hardness, underscoring the potential of LPBF for cost-effective and customizable ceramic component manufacturing.

Keywords: Laser powder bed fusion; Selective laser melting; Silicon carbide; Ultra-fast heating; High-speed temperature scanner; Reactive sintering

***Corresponding author:** Tsovinar Ghaltaghchyan (tsovinar.ghaltaghchyan@ichph.sci.am)

Citation: Ghaltaghchyan T, Nazaretyan K, Khachikyan A, Aghayan M. Reactive selective laser melting of silicon carbide. *Mater Sci Add Manuf*. 2026;5(1):025340079. doi: 10.36922/MSAM025340079

Received: August 22, 2025

Revised: September 18, 2025

Accepted: September 24, 2025

Published online: October 31, 2025

1. Introduction

Silicon carbide (SiC) is an advanced ceramic with high hardness, strength, thermal conductivity, and chemical stability, making it suitable for cutting tools, armor, aerospace components, and electronics.[1] Conventional manufacturing methods, such as dry pressing,[2] slip casting,[3] tape casting,[4] and injection molding,[5] enable achieving high performance of ceramic; however, machining to obtain more complex geometries is challenging. Ceramics have poor machining performance because of their brittleness, low shear strength, and excessive tool wear.[6,7] Therefore, the production of components with near-net-shape designs is crucial.

Recent advances in laser powder bed fusion (LPBF) technologies have enabled the successful fabrication of high-performance metallic materials with tailored microstructures and mechanical properties.[8-10] These techniques have demonstrated notable achievements in producing dense, defect-minimized components with superior strength and hardness. However, despite such successes in metals, the application of

these AM methods of SiC remains highly challenging due to its high melting point,[11] intrinsic brittleness, and low fracture toughness.[12] Most reported SiC-based materials rely on complex, high-temperature sintering, which limits scalability and compatibility with AM.

Recently, AM of SiC has garnered the attention of industrial leaders and researchers. Considering that the mechanical properties of the ceramic are a sign of its defects, many researchers focused on improving the strength of SiC. Table 1 summarizes different AM and traditional techniques to manufacture SiC.

Although the post-processing of additive-manufactured samples plays a crucial role in the density and mechanical properties thereof,[17] this technology has not yet achieved the production of fully defect-free components. Overall, traditional manufacturing technologies result in higher density and sometimes significantly higher mechanical properties than AM. Consequently, there is a clear research gap in developing processing routes for SiC-based systems that can deliver competitive mechanical performance while being more time-efficient, cost-effective, and environmentally friendly.

The present work responds to this challenge by exploiting the advantages provided by LPBF, in addition to its high geometric flexibility and the ability to fabricate complex near-net-shape components directly from digital models.[26,27] This design freedom is particularly significant for ceramics and composites, where conventional shaping methods are constrained by brittleness and strict processing requirements.[28,29]

However, ceramics are generally challenging to process via laser-based AM.[30] Several studies have reported varying outcomes depending on the feedstock and process parameters. Meyers[31] produced SiC parts with ~95% relative density by LPBF using a mixture of 67 wt% SiC and 33 wt% Si, followed by carbon impregnation and molten silicon infiltration.[31] Zou *et al.*[32] used SiC with short carbon fibers, followed by two-stage carbonization and silicon infiltration.

Ghaltaghchyan *et al.*[33] fabricated SiC preforms via direct LPBF using a bimodal mixture of SiC, Si, and hexagonal boron nitride, which reached up to 87% relative density and a Young's modulus of 59.8 ± 0.3 GPa without post-processing.[33] These studies highlight the importance of feedstock selection, process parameters, and heating rates in achieving high-density, mechanically robust SiC parts.

This article aims to present a novel approach for manufacturing SiC using selective laser melting within LPBF technologies. In this method, the feedstock containing silicon and activated carbon is rapidly heated by the laser beam, promoting the *in situ* formation of SiC within the printer's chamber. The process consolidates material layer by layer while simultaneously enabling chemical reactions between the constituent powders, effectively combining AM with *in situ* reactive phase formation.

The influence of LPBF process parameters on SiC formation was investigated. The effect of boron carbide (B_4C) on reactions and subsequent post-processing was studied. This is the first study to apply an ultra-high heating rate of 3400°C/min during post-processing of the LPBF-printed samples for the purposes of enhancing Si–C reaction and densification.

2. Materials and methods

2.1. Powder feedstock preparation

The first powder feedstock (Feed 1) was prepared using silicon powder (microcut <20 µm; SILGRAIN, Elkem ASA, Norway) mixed with activated carbon (Lach: ner, Czech Republic). The second feedstock (Feed 2) was obtained by adding 5 wt.% B_4C (particle size 1–7 µm, purity >98%; Sigma Aldrich, Germany) powder into the Feed 1 as a sintering additive. The composition of both feedstocks is presented in Table 2.

In Feed 1, a slightly higher fraction of silicon was used, compared to stoichiometric calculations, to ensure complete reaction with carbon and to compensate for potential losses or incomplete conversion during the rapid laser heating process. This excess of silicon facilitates the formation of dense SiC while minimizing residual unreacted carbon.

Initial powders were mixed in acetone using a magnetic stirrer for 30 min inside a closed jar. The lid of the jar was then removed, and the stirrer was heated while stirring continued to facilitate the drying of the feedstock. The final drying of powder was performed in the forced air-drying oven WGLL-65BE series (FAITHFUL, China) at 80°C for 3 h.

2.2. LPBF

The solid samples were built with dimensions of 10 × 10 × 5 mm. The LPBF process was carried out in a pure argon environment with an oxygen level kept below 0.1%. The printing parameters were systematically varied to identify the optimal process window. Parameter optimization was based on multiple output responses, including visual inspection for macroscopic defects, X-ray diffraction (XRD) analysis to assess phase composition (SiC-to-Si ratio), and practical considerations such as energy efficiency and processing stability.

Macroscopic quality was first assessed through visual inspection, focusing on surface integrity, the presence

Table 1. Various techniques for SiC processing

Composition	Method of sintering and conditions	Density and porosity	Mechanical properties	References
Si+α-SiC	Direct laser sintering+phenolic resin infiltration with liquid silicon infiltration	Up to 84% SiC content	Young's modulus: 285±5 GPa Flexural strength: 162±7 MPa Hardness: 2045±252 HV	13
SiC+Si	Direct laser powder bed fusion with chemical vapor infiltration	78.3%	Compressive strength: 90±8 MPa	14
Whisker-reinforced SiC	Binder jetting and chemical vapor infiltration	2.77 g/cm^3	Flexural strength: 200 MPa Fracture toughness: 3.4 MPa m$^{1/2}$ Elastic modulus (with nanoindentation): 458 GPa	15
SiC	Selective laser sintering+precursor infiltration and pyrolysis	2.59 g/cm^3	Flexural strength: 220 MPa	16
SiC+10 wt.% Al_2O_3–Y_2O_3	Stereolithography+liquid phase sintering	78.2±1.36%	Flexural strength: 77±5.2 MPa	17
SiC	Stereolithography+precursor infiltration and pyrolysis	82.6±0.48%	Flexural strength: 184.2±8.5 MPa	17
SiC+Si powder	Stereolithography+liquid silicon infiltration	96.2±0.32%	Flexural strength: 210.4±10.3 MPa	17
SiC+Si (5.2 vol.%)	Binder jetting	2.89 g/cm^3	Flexural strength: 385±25 MPa Fracture toughness: 5.93±0.32 MPa m$^{1/2}$	18
SiC	Spark plasma sintering, 2050°C	3.187 g/cm^3	Young's modulus: 440±20 GPa Flexural strength: 490±70 MPa Hardness: 20±2 GPa to 32±0.7 GPa	19
SiC+1.65 wt% Al	Hot pressing, 28 MPa, 2100°C	3.20–3.21 g/cm^3	Hardness: 24.6±0.5 HV1 (GPa) Strength: 705±63 MPa	20
SiC+2.52 wt.% AlN			Hardness: 23.3±0.3 HV1 (GPa) Strength: 640±100 MPa	
SiC+1 wt.% C+0.25 wt.% B_4C			Hardness: 26.9±1.0 HV1 (GPa) Strength: 447±113 MPa	
SiC+α-Al_2O_3+graphite	Bidirectionally pressing, sintering in air, 1400–1550°C	Open porosity of 43.4%	Flexural strength: 24.0 MPa	21
SiC+carbon black	Reaction bonding with molten silicon at 1600°C, 20 min under vacuum	<50%, 2.85 g/cm^3	Flexure strength: 260±50 MPa to 310±40 MPa	22
SiC+B_4C	Uniaxially compacting under 180 MPa, infiltrated with liquid silicon at 1480°C	2.79–2.92 g/cm^3	Young's modulus: 343–353 GPa Flexural strength: 171–270 MPa Hardness: 1534±202 to 1963±331 HV	23
Amorphous carbon black+micro-spherical carbon+molten Si	Uniaxial die-pressing at 80 MPa for 60 s, thermal treatment at 1550–1850°C	3.14 g/cm^3	Young's modulus: 443 GPa Hardness: 25.3 GPa	24
SiC+paraffin-based binder	Injection to a mold, thermal debinding, four times impregnation with phenolic resin and pyrolysis, and infiltration with silicon	3.14±0.02 g/cm^3	Flexural strength: 225±52 MPa	25

of cracks, and signs of warping. Phase composition was evaluated using XRD analysis to determine the SiC-to-Si ratio and to identify any potential decomposition or formation of secondary phases. Processing stability includes build repeatability and powder recoating behavior during fabrication. Finally, energy input was optimized to avoid excessive overheating or material degradation while still achieving adequate densification. These combined

factors were used to identify the most effective and reliable set of processing parameters. Table 3 summarizes the main printing parameters applied for the consolidation of powders.

2.3. Heat treatment

The high-speed temperature scanner (HSTS) technique was used to heat the printed samples.[34] Each sample was enclosed in a carbon envelope, which was heated directly by an electrical current, following a programmed temperature schedule managed by a PC-assisted controller. The heating process occurred in an argon-protective atmosphere at a controlled heating rate. The samples were heated at a rate of 3400°C/min up to 1730°C and cooled down at 100°C/min. The dwell time was 3 min.

The selected sintering temperature of 1730°C was chosen considering the melting point of silicon (~1410°C),[35] to ensure the formation of liquid silicon and thereby promote its reaction with carbon to form SiC. The sintering temperature was kept below the decomposition temperature of SiC.

The chosen maximum heating rate of 3400°C/min for the HSTS setup was based on our earlier research, which showed that elevated heating rates enhance SiC formation.[36] Under slow heating conditions, the initially formed SiC layer acts as a diffusion barrier between silicon and carbon powders, hindering further reaction. Rapid heating reduces this effect by promoting more uniform reaction throughout the entire material.

These parameters were selected to promote rapid Si–C reaction and densification while reducing excessive grain growth, secondary phase formation, or thermal damage to the preforms.

The temperature of the samples was monitored using tungsten-rhenium thermocouples positioned at the center of each sample. The thermocouples' output signals were processed through a multichannel acquisition system and logged by a computer. Throughout the process, both the temperature profile and the applied current were continuously documented.

Table 2. Composition of raw powders for LPBF printing

Feedstock number	Composition
Feed 1	Si (72 wt.%)+C (28 wt.%)
Feed 2	Si (68.4 wt.%)+C (26.6 wt.%)+B_4C (5 wt.%)

Abbreviation: LPBF: Laser powder bed fusion.

Table 3. The main printing parameters for the LPBF process

Printing parameters	Values tested in experiments	Optimized values
Laser power (W)	30–50	48
Powder layer thickness (μm)	25–35	35
Hatch distance (μm)	60–80	60
Focal length of the focusing lens (mm)	4; 9.8; 14	4
Rotation between layers (°)	60; 90	60
Exposure time (μs)	40; 80; 120; 160	40
Point distance (μm)	5–15	5
Baseplate material	Ti, SiC	SiC
Heating of baseplate (°C)	RT; 100; 150	100

Abbreviations: LPBF: Laser powder bed fusion; RT: Room temperature.

2.4. Characterization

To examine the porosity and microstructural characteristics, the produced rectangular samples were put in epoxy resin, cross-sectioned, and polished in the direction perpendicular to the printing plane. The universal grinding and polishing device was applied (Qpol GO model, Mammelzen, Germany).

A scanning electron microscope (SEM; Prisma E, Thermo Fisher Scientific, Hillsboro, OR, USA), equipped with an energy dispersive spectroscopy detector, was employed. Samples were subjected to coating with a thin layer of gold to provide sufficient conductivity.

The composition of the samples after the printing and heat treatment was determined by means of XRD using a Mini Flex 600 X-ray Diffractometer (Rigaku, Japan) with these settings: 40 mA, 40 kV, Cu Kα radiation, $\lambda = 0.1542$ nm, and a step size of 0.02°. The samples were broken and ground for analysis.

The Vickers hardness of the heat-treated samples was measured using FALCON 600G2FA Automated Hardness Testing System (INNOVATEST Europe BV, Maastricht, Netherlands). The indenter has a square base with a 136° angle between opposite faces. The load applied to the indenter was 0.2 kgf.

The carbon concentration in feedstock and samples was measured through combustion in an induction furnace above 2000°C in the presence of oxygen and a catalyst. This converts the element into gaseous CO_2, which was then separated and measured sequentially by infrared absorption. The elemental analyzer ELEMENTRAC CS (ELTRA Elemental Analyzers, Germany) was used in this regard.

3. Results and discussion

3.1. Feedstock characterization

The flowability of the feedstock powders has a significant impact on their distribution on the LPBF printing platform.

The flowability is influenced by the size and form of the particles. Microstructural analysis indicates that both final powder mixture particles contained angular structures and did not exhibit aggregation (Figure 1).

The powders were not as spherical as preferred for ideal flowability; however, mixing within the acetone environment positively influenced the powder distribution in a 2D layer. It is assumed that acetone acts as a dispersing agent, reducing interparticle forces and preventing agglomeration of fine particles during mixing. This results in a more uniform microscale distribution of silicon and carbon powders, improving feedstock homogeneity. Moreover, wet mixing also breaks down soft agglomerates that persist in dry mixing, and after solvent evaporation, a finely dispersed powder with reduced clustering is obtained, enhancing powder flow and layer uniformity.

Although spherical powders are generally preferred in LPBF due to superior flowability and packing density, angular powders can provide unique benefits for processing ceramics. The irregular geometry of angular particles promotes multiple internal reflections of the incident laser beam on the particle surfaces. This effect enhances light absorption compared to smooth, spherical powders, which is particularly advantageous for highly reflective ceramic systems such as silicon and SiC.[37] Ultimately, a balanced feedstock structure was obtained, where the non-spherical particles enabled uniform spreading on the baseplate and provided adequate absorptivity and sinterability for efficient LPBF processing.

The powder mixtures were processed using selective laser melting, a unique technique under the umbrella of LPBF. Powder distribution on the building platform was assessed visually. In case of local accumulation of powder, the platform height and the tension of the leveling rubbers on the wiper were adjusted. After the adjustments, printing was conducted in a pure argon atmosphere to prevent oxidation.

The elemental analysis indicates that the carbon content in Feeds 1 and 2 is 21% and 20%, respectively. These are slightly lower than the carbon content in a raw material (Table 2).

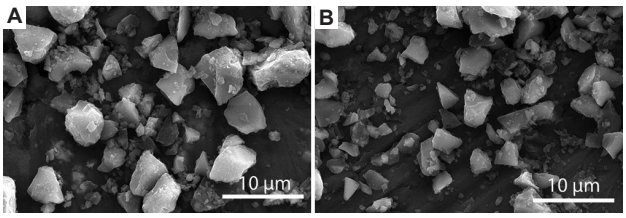

Figure 1. SEM images of final raw powders—Feed 1 (A) and Feed 2 (B)—at high magnification (10 000×)
Abbreviation: SEM: Scanning electron microscopy

3.2. LPBF

Laser power was identified as a critical parameter governing the printing process. At powers below 31 W, only partial sintering occurred, yielding highly brittle samples that disintegrated upon removal from the platform. Conversely, powers above 48 W led to excessive energy input, causing sparking, smoke generation, and the formation of brittle parts. Hence, the range of 31–48 W was established as optimal for stable fabrication. The influence of sintering agents, particularly B_4C, on the sinterability and silicon-carbon reaction was investigated, too. The complete set of samples fabricated by LPBF is summarized in Table 4.

3.3. Effect of laser focus and exposure time

Exposure time was varied between 40 and 160 µs to optimize energy input. Although XRD showed a modest increase in the SiC/Si ratio with higher exposure times (Figure 2B), the improvement was limited, and 40 µs was therefore considered sufficient to balance productivity and SiC formation.

Compared to exposure time, focal length had a stronger influence. According to Equation I, increasing the focal length enlarges the spot size, thereby reducing energy density.

$$d_s = 4\lambda f/\pi D \quad (I)$$

where d_s represents spot size (diameter of the laser beam at the focal point); λ represents laser wavelength; f represents focal length of the focusing lens; and D represents

Table 4. List of LPBF-printed samples

Sample ID	Composition	Laser power (W)	Focal length (mm)	Exposure time (µs)	Post-processing
S1	Feed 1	31	4	40	No
S2	Feed 1	36	4	40	No
S3	Feed 1	48	4	40	No
S2H	Feed 1	36	4	40	Yes
S3H	Feed 1	48	4	40	Yes
S4	Feed 1	48	9.8	40	No
S5	Feed 1	48	9.8	80	No
S6	Feed 1	48	9.8	160	No
S7	Feed 1	48	14	40	No
S8	Feed 2	31	4	40	No
S9	Feed 2	36	4	40	No
S10	Feed 2	48	4	40	No
S9H	Feed 2	36	4	40	Yes
S10H	Feed 2	48	4	40	Yes

Abbreviation: LPBF: Laser powder bed fusion.

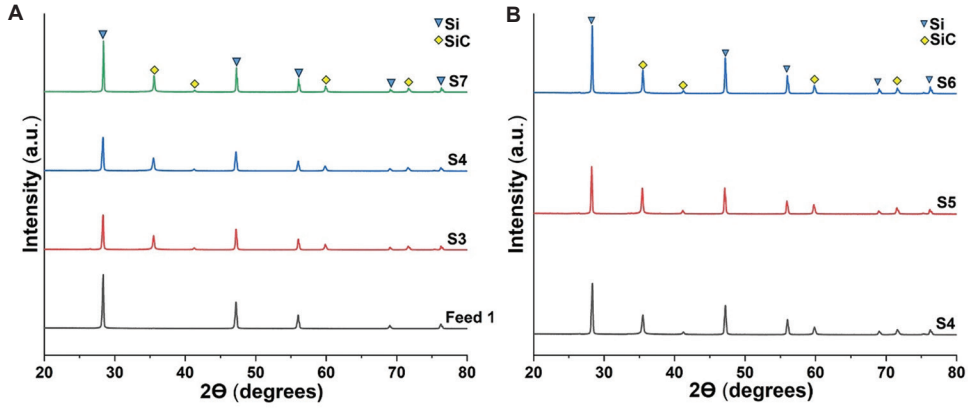

Figure 2. XRD analysis of LPBF-printed samples at different focal length (A) and exposure time (B)
Abbreviations: LPBF: Laser powder bed fusion; XRD: X-ray diffraction

input beam diameter before focusing. Therefore, a longer focal length results in a larger spot size. Reducing the focal length from 14 mm to 4 mm increased local energy input, which enhanced the SiC-to-Si ratio (Figure 2A).

3.4. Effect of B_4C as a sintering agent

The influence of B_4C on the microstructure of LPBF-printed samples was studied. The cross-sections of the samples S3 and S10 are illustrated in Figure 3.

SiC-based ceramic was chosen as the substrate of all the samples, due to its ability to enhance adhesion of the feedstock. Figure 3A illustrates the microstructure of the LPBF-printed sample S3 using Feed 1. The as-obtained SiC–Si grains had elongated structures with different sizes. However, the sintering process left enormous pores in the samples. Adding 5 wt.% B_4C led to reduced porosity (Figure 3B). Overall, the samples (S8, S9, S10) containing B_4C in the feedstock (Feed 2) exhibited a more uniform structure with fewer pores compared to the feedstock without an additive. Moreover, B_4C enhanced carbidization of silicon. XRD analysis showed that the Si-to-SiC ratio decreases when using B_4C in the feedstock (S9 and S10) compared with the B_4C-free samples (S2, S3) (Figure 3C). As it has been mentioned in the literature, the incorporation of B_4C changes the microstructure and reaction kinetics of SiC.[38] During the reactive sintering process, boron–silicon–carbon liquid phase forms, which enhances both the sintering of SiC and its formation.[39,40]

The Redfield analysis showed that the obtained SiC content in the printed samples (S1, S2, S3) was ~45 %. Thus, this indicates that raising laser power from 31 W to 48 W does not influence the rate of interaction between Si and C when Feed 1 is utilized. However, samples containing B_4C (S8, S9, and S10) show another behavior. The increased amount of SiC from 50% to 55% necessitated

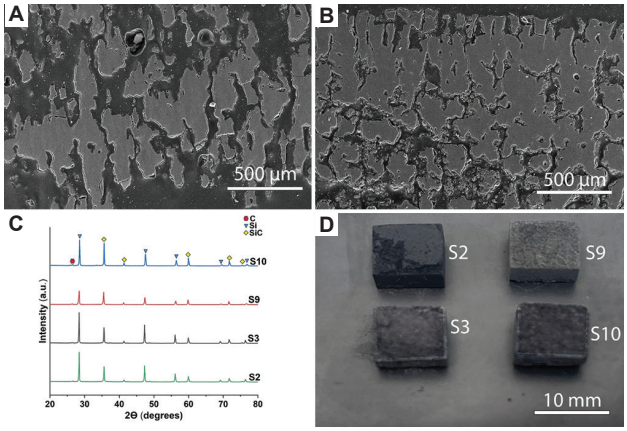

Figure 3. The samples after LPBF printing using Feed 1 and Feed 2. (A) Microstructure of S3; (B) Microstructure of S10; (C) XRD analysis of S2, S3, S9, and S10; (D) LPBF-printed samples. Magnification: 200× (A–B)
Abbreviations: LPBF: Laser powder bed fusion; XRD: X-ray diffraction

a laser power increase from 31 W to 36 W (in S8 and S9, respectively). The further increase of laser power to 48 W does not influence the SiC content (in S10). In all of these cases, it was possible to obtain samples with clearly defined contours (Figure 3D).

Although the SiC fraction achieved in this study reached ~55%, with residual silicon remaining after post-printing heat treatment. Residual silicon can compromise high-temperature performance, including thermal stability and oxidation resistance, significantly limiting the material's maximum service temperature and restricting its use in harsh environments.[38] However, it can also enhance machinability in certain applications. For applications requiring high thermal or chemical stability, strategies to further increase SiC formation are necessary.

Future experiments will focus on maximizing SiC formation by combining extended dwell times, multi-step

heating protocols (controlled pre-heating stages and ramp rates), and optimized feedstock composition with potential sintering aids. These strategies are expected to enhance Si–C reaction kinetics, promote uniform SiC growth, and achieve higher carbidization levels in the printed samples.

Another limitation is the discrepancy between the intended and actual carbon content in the feedstock. This reduction likely arises from the partial loss of fine carbon particles during wet mixing, drying, and handling, which prevented the full incorporation of the initially added carbon into the final powder mixture. The lower carbon content may have limited the Si–C reaction, reducing the final SiC fraction and influencing the microstructure and hardness of the printed samples. Consequently, the presented results may underestimate the maximum achievable SiC formation under the selected processing conditions.

Compared to the literature reported in Table 1, where SiC densification typically requires multi-step infiltration or hot pressing, our results highlight that direct LPBF with B_4C achieves comparable SiC formation in a single step, albeit with some residual porosity.

3.5. Heat treatment of LPBF-printed samples

Our previous research demonstrated that the heating rate strongly influences the Si–C reaction mechanism and yield.[36] At high heating rates, silicon melts and wets the carbon surface before a continuous SiC layer can form, thereby accelerating Si–C interaction. Figure 4 presents the microstructure and XRD patterns of heat-treated samples (S2H, S3H, S9H, and S10H).

Microstructural analysis revealed that the samples consisted of silicon, SiC, and pores. Samples without B_4C exhibited a heterogeneous microstructure, characterized by unevenly distributed fine SiC grains within the silicon matrix (Figure 4A and B). Samples produced at higher laser power (S3H and S10H, at 48 W) were less homogeneous compared to those fabricated at lower power (S2H and S9H). XRD and SEM analyses confirmed that the highest SiC content was obtained in sample S9H, which contained B_4C and was processed at 36 W (Figure 4C and E). At higher power (for S10H), coarser SiC grains were observed (Figure 4D), although the overall SiC content was lower than in sample S9H.

During the LPBF process, silicon reacts with carbon to form SiC. However, the initially formed SiC may act as a diffusion barrier, limiting further carbidization during subsequent heat treatment. At higher laser powers, larger amounts of SiC were generated, and post-treatment primarily promoted the growth and coarsening of existing SiC grains (Figure 4D). In contrast, post-heat treatment of sample S9 facilitated additional Si–C interaction, leading to the nucleation of new SiC grains and the enlargement of pre-existing ones.

These results indicated that B_4C not only facilitates the Si–C reaction but also improves microstructural uniformity. This observation is consistent with earlier reports that B_4C promotes transient B–Si–C liquid phase formation, enhancing diffusion and carbidization efficiency.[40,41] Furthermore, our results demonstrate that excessive laser energy input can promote grain coarsening and reduce effective SiC yield, in line with literature on laser processing, where localized overheating is known to limit densification by promoting exaggerated grain growth.[42]

Compared to conventional sintering or infiltration-based approaches, where SiC densification often requires prolonged thermal treatments at >2000°C,[43,44] the combined effect of B_4C addition and optimized laser power in our study enabled significant SiC formation and improved microstructural

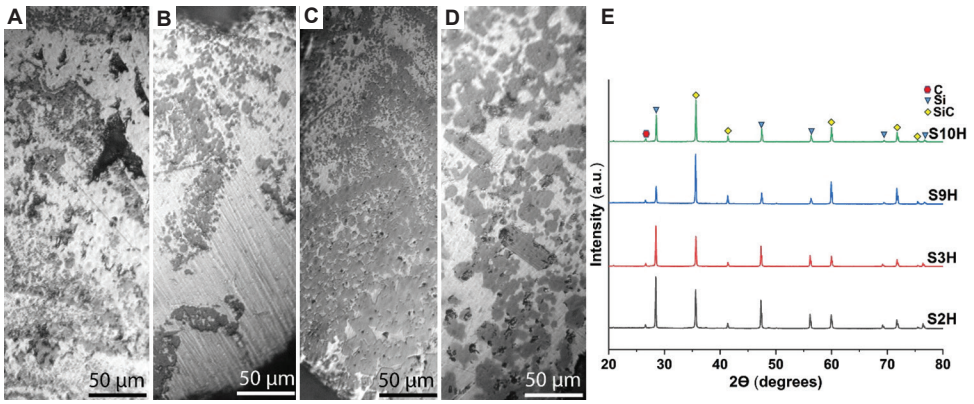

Figure 4. The LPBF-printed samples following heat treatment at a rate of 3400°C/min up to 1730°C (A–D) and XRD analysis of these samples (E). (A) Microstructure of S2H; (B) Microstructure of S3H; (C) Microstructure of S9H; (D) Microstructure of S10H; (E) XRD analysis of S2H, S3H, S9H, and S10H. Magnification: 50× (A–D)
Abbreviations: LPBF: Laser powder bed fusion; XRD: X-ray diffraction

quality at relatively lower processing temperatures. This highlights the potential of direct LPBF combined with reactive agents for producing SiC-based materials with tailored microstructures in a single-step process.

The Vickers hardness values of samples S2H, S3H, S9H, and S10H, measured with a 0.2 kgf load, were 1168, 933, 1091, and 1218, respectively. Indentations were performed on SiC grains. Among them, sample S10H exhibited the highest hardness, which can be attributed to the coarse SiC grain size. Since the SiC grains are embedded in a silicon matrix, the measured hardness values may be lower than those of pure SiC. A similar observation was reported by Chaugule *et al.*,[45] who showed that in 3D-printed Si–SiC composites, the hardness of the silicon regions was nearly half that of the SiC regions.[45] In our case, the smaller SiC grain size and the surrounding silicon phase likely contributed to the measured hardness values.

For comparison, the hardness of dense monolithic SiC typically exceeds 2000 HV, depending on grain size and processing route.[46,47] The lower values obtained in this work can be explained by the presence of residual silicon and porosity, which reduce the effective hardness of the composite microstructure. Nevertheless, the achieved hardness values fall within the range reported for reaction-bonded Si–SiC systems, highlighting the potential of LPBF combined with post-treatment for fabricating mechanically robust SiC-based parts.

4. Conclusion

LPBF of SiC from silicon and carbon powders was successfully performed. The effects of printing parameters and the addition of B_4C on the process yield were systematically investigated. As-fabricated samples contained up to 55 % SiC, with B_4C promoting the carbidization of silicon during the LPBF process.

The printed samples were subjected to fast heat treatment, with a heating rate of 3400°C/min up to 1730°C and a dwell time of 3 min. Enhanced carbidization was observed in B_4C-containing samples produced at lower laser power. After heat treatment, samples containing B_4C printed at higher laser power exhibited larger SiC grains and achieved the highest Vickers hardness of 1218 $HV_{0.2}$.

Acknowledgments

None.

Funding

This work was supported by the Higher Education and Science Committee of MESCS RA under grant numbers 22AA-2F022 and 22IRF-05.

Conflict of interest

The authors declare they have no competing interests.

Author contributions

Conceptualization: Marina Aghayan
Formal analysis: Ani Khachikyan
Investigation: Tsovinar Ghaltaghchyan, Khachik Nazaretyan
Methodology: Marina Aghayan, Tsovinar Ghaltaghchyan
Writing–original draft: Tsovinar Ghaltaghchyan
Writing–review & editing: Marina Aghayan

Ethics approval and consent to participate

Not applicable.

Consent for publication

Not applicable.

Availability of data

All raw data generated and analyzed during this study are stored in the personal research storage of the corresponding author. These data are not publicly available due to internal storage policy but can be provided by the author upon reasonable request for further verification or processing related to the article.

Further disclosure

Findings included in this article were previously presented as a poster at the "*Materials Today 2025*" conference, held on June 23–26, 2025 at Sitges, Spain.

References

1. Izhevskyi VA, Genova LA, Bressiani JC, Bressiani AHA. Review article: Silicon carbide. Structure, properties and processing. *Cerâmica*. 2000;46(297):4-13.

   doi: 10.1590/S0366-69132000000100002

2. Freedman MR, Millard ML. Improved consolidation of silicon carbide. In: *10th Annual Conference on Composites and Advanced Ceramic Materials: Ceramic Engineering and Science Proceedings*. Vol. 7. United States: John Wiley & Sons, Inc.; 1986. p. 884-892.

   doi: 10.1002/9780470320341.ch15

3. Frolova MG, Leonov AV, Kargin Yu F, *et al.* Molding features of silicon carbide products by the method of hot slip casting. *Inorgan Mater Appl Res*. 2018;9(4):675-678.

   doi: 10.1134/S2075113318040123

4. Luo ZH, Jiang DL, Zhang JX, Lin QL, Chen ZM, Huang ZR. Preparation of reaction-bonded silicon carbide with well controlled structure by tape casting method. *Ceram Int*.

2012;38(3):2125-2128.

doi: 10.1016/j.ceramint.2011.10.053

5. Zhang Z, Zhang Y, Gong H, *et al*. Influence of carbon content on ceramic injection molding of reaction-bonded silicon carbide. *Int J Appl Ceram Technol*. 2016;13(5):838-843.

doi: 10.1111/ijac.12570

6. Bharathi V, Anilchandra AR, Sangam SS, Shreyas S, Shankar SB. A review on the challenges in machining of ceramics. *Mater Today Proc*. 2021;46:1451-1458.

doi: 10.1016/j.matpr.2021.03.019

7. Sharma D, Khurana M, Manghnani S, Chhatrawat RS, Goswami C, Yadav AK. The Challenges in Machining of Ceramics- A Short Review. In: *Proceedings of the Advancement in Electronics and Communication Engineering*; 2022. Available from: https://ssrn.com/abstract=4186512 [Last accessed on 2025 Oct 15].

8. Niu Z, Zhang J, Liu F, *et al*. Forming quality control of laser powder bed fusion GH3536 alloy: Surface quality, defects, and microstructure. *Mater Sci Addit Manuf*. 2025;4(4):025220042.

doi: 10.36922/MSAM025220042

9. Lu Z, San SLL, Tan MJ, An J, Zhang Y, Chua CK. Preliminary investigation on tensile and fatigue properties of Ti6Al4V manufactured by selected laser melting. *Mater Sci Addit Manuf*. 2023;2(2):0912.

doi: 10.36922/msam.0912

10. Gunasekaran J, Sevvel P, John Solomon I. Metallic materials fabrication by selective laser melting: A review. *Mater Today Proc*. 2021;37:252-256.

doi: 10.1016/j.matpr.2020.05.162

11. Langpoklakpam C, Liu AC, Chu KH, *et al*. Review of silicon carbide processing for power MOSFET. *Crystals (Basel)*. 2022;12(2):245.

doi: 10.3390/cryst12020245

12. Fan Z, Zhang J, Wang Z, Shan C, Huang C, Wang F. A state-of-the-art review of fracture toughness of silicon carbide: Implications for high-precision laser dicing techniques. *Processes*. 2024;12(12):2696.

doi: 10.3390/pr12122696

13. Meyers S, De Leersnijder L, Vleugels J, Kruth JP. Direct laser sintering of reaction bonded silicon carbide with low residual silicon content. *J Eur Ceram Soc*. 2018;38(11):3709-3717.

doi: 10.1016/j.jeurceramsoc.2018.04.055

14. Wang Y, Wang P, Li L, *et al*. Effect of Si addition on microstructure and mechanical properties of SiC ceramic fabricated by direct LPBF with CVI technology. *Applied Sciences*. 2025;15(15):8585.

doi: 10.3390/app15158585

15. Lv X, Ye F, Cheng L, Fan S, Liu Y. Fabrication of SiC whisker-reinforced SiC ceramic matrix composites based on 3D printing and chemical vapor infiltration technology. *J Eur Ceram Soc*. 2019;39(11):3380-3386.

doi: 10.1016/j.jeurceramsoc.2019.04.043

16. Xu T, Cheng S, Jin L, Zhang K, Zeng T. High-temperature flexural strength of SiC ceramics prepared by additive manufacturing. *Int J Appl Ceram Technol*. 2020;17(2):438-448.

doi: 10.1111/ijac.13454

17. Bai X, Ding G, Zhang K, *et al*. Stereolithography additive manufacturing and sintering approaches of SiC ceramics. *Open Ceramics*. 2021;5:100046.

doi: 10.1016/j.oceram.2020.100046

18. Lv X, Gao L, Cui X, *et al*. Binder jetting additive manufacturing of hierarchical structural SiCw/SiC composites. *Addit Manuf*. 2024;93:104434.

doi: 10.1016/j.addma.2024.104434

19. Hayun S, Paris V, Mitrani R, *et al*. Microstructure and mechanical properties of silicon carbide processed by Spark Plasma Sintering (SPS). *Ceram Int*. 2012;38(8):6335-6340.

doi: 10.1016/j.ceramint.2012.05.003

20. Ray DA, Kaur S, Cutler RA, Shetty DK. Effect of additives on the activation energy for sintering of silicon carbide. *J Am Ceramic Soc*. 2008;91(4):1135-1140.

doi: 10.1111/j.1551-2916.2008.02271.x

21. Ding S, Zhu S, Zeng YP, Jiang D. Fabrication of mullite-bonded porous silicon carbide ceramics by *in situ* reaction bonding. *J Eur Ceram Soc*. 2007;27(4):2095-2102.

doi: 10.1016/j.jeurceramsoc.2006.06.003

22. Paik U, Park HC, Choi SC, Ha CG, Kim JW, Jung YG. Effect of particle dispersion on microstructure and strength of reaction-bonded silicon carbide. *Mater Sci Eng A*. 2002;334(1-2):267-274.

doi: 10.1016/S0921-5093(01)01897-4

23. Aroati S, Cafri M, Dilman H, Dariel MP, Frage N. Preparation of reaction bonded silicon carbide (RBSC) using boron carbide as an alternative source of carbon. *J Eur Ceram Soc*. 2011;31(5):841-845.

doi: 10.1016/j.jeurceramsoc.2010.11.032

24. Zhang NL, Yang JF, Deng YC, Wang B, Yin P. Preparation and properties of reaction bonded silicon carbide (RB-SiC) ceramics with high SiC percentage by two-step sintering using compound carbon sources. *Ceram Int*. 2019;45(12):15715-15719.

doi: 10.1016/j.ceramint.2019.04.224

25. Grinchuk PS, Kiyashko MV, Abuhimd HM, *et al*. Advanced technology for fabrication of reaction-bonded SiC with controlled composition and properties. *J Eur Ceram Soc*.

2021;41(12):5813-5824.

doi: 10.1016/j.jeurceramsoc.2021.05.017

26. Grant GT. Direct digital manufacturing. In: *Clinical Applications of Digital Dental Technology*. United States: Wiley; 2023. p. 46-59.

doi: 10.1002/9781119800613.ch3

27. Hopkinson N, Hague RJM, Dickens PM, editors. *Rapid Manufacturing*. United States: Wiley; 2005.

doi: 10.1002/0470033991

28. Gavalda-Diaz O, Saiz E, Chevalier J, Bouville F. Toughening of ceramics and ceramic composites through microstructure engineering: A review. *Int Mater Rev*. 2025;70(1):3-30.

doi: 10.1177/09506608241308337

29. Karadimas G, Salonitis K. Ceramic matrix composites for aero engine applications-a review. *Appl Sci*. 2023;13(5):3017.

doi: 10.3390/app13053017

30. Ur Rehman A, Saleem MA, Liu T, Zhang K, Pitir F, Salamci MU. Influence of silicon carbide on direct powder bed selective laser process (sintering/melting) of alumina. *Materials*. 2022;15(2):637.

doi: 10.3390/ma15020637

31. Meyers S. *Direct Selective Laser Sintering of Reaction Bonded Silicon Carbide*. Available from: https://hdl.handle.net/2152/89454 [Last accessed on 2025 Oct 10].

32. Zou Y, Li CH, Tang Y, *et al*. Preform impregnation to optimize the properties and microstructure of RB-SiC prepared with laser sintering and reactive melt infiltration. *J Eur Ceram Soc*. 2020;40(15):5186-5195.

doi: 10.1016/j.jeurceramsoc.2020.07.023

33. Ghaltaghchyan T, Khachatryan H, Asatryan K, Rstakyan V, Aghayan M. Effect of additives on selective laser sintering of silicon carbide. *Bol Soc Esp Cerám Vidrio*. 2023;62(6):504-514.

doi: 10.1016/j.bsecv.2023.01.001

34. Zakaryan M, Nazaretyan K, Aydinyan S, Kharatyan S. Joint reduction of NiO/WO3 pair and NiWO4 by Mg + C combined reducer at high heating rates. *Metals (Basel)*. 2021;11(9):1351.

doi: 10.3390/met11091351

35. Gayler ML. Melting point of high-purity silicon. *Nature*. 1938;142(3593):478-478.

doi: 10.1038/142478a0

36. Ghaltaghchyan T, Nazaretyan K, Rstakyan V, Aghayan M. Fast carbidization of silicon in additive manufactured Si-C-SiC composite. Results Mater. 2025;25:100653.

doi: 10.1016/j.rinma.2024.100653

37. Gu D, Yang Y, Xi L, Yang J, Xia M. Laser absorption behavior of randomly packed powder-bed during selective laser melting of SiC and TiB2 reinforced Al matrix composites. *Opt Laser Technol*. 2019;119:105600.

doi: 10.1016/j.optlastec.2019.105600

38. Liu R, Chen G, Qiu Y, *et al*. Fabrication of porous SiC by direct selective laser sintering effect of boron carbide. *Metals (Basel)*. 2021;11(5):737.

doi: 10.3390/met11050737

39. Stobierski L, Gubernat A. Sintering of silicon carbide II. Effect of boron. *Ceram Int*. 2003;29(4):355-361.

doi: 10.1016/S0272-8842(02)00144-X

40. Chen J, Chen P, Li X, Zhu Y, Wang F. Effect of B4C on the microstructure and mechanical properties of SiC refractory ceramics. 2022. Available from: https://www.researchgate.net/publication/363930570_Effect_of_B4C_on_the_Microstructure_and_Mechanical_Properties_of_SiC_Refractory_Ceramics [Last accessed on 2025 Oct 10].

41. Stobierski L, Gubernat A. Sintering of silicon carbide I. Effect of carbon. *Ceram Int*. 2003;29(3):287-292.

doi: 10.1016/S0272-8842(02)00117-7

42. Fang J, Tan YC, Yang Y, *et al*. Influence of laser power on microstructure and performance of SiC/Ti composite fabricated through selective laser melting. *J Mater Res Technol*. 2025;34:1130-1143.

doi: 10.1016/j.jmrt.2024.12.044

43. Lee EJ, Lee DH, Kim JC, Kim DJ. Densification behavior of high purity SiC by hot pressing. *Ceram Int*. 2014;40(10):16389-16392.

doi: 10.1016/j.ceramint.2014.07.143

44. Shin S, Kim M, Kim M, *et al*. Ultrafast high-temperature sintering of reaction-bonded SiC with Y2O3-Al2O3 sintering additives. *Mater Lett*. 2025;382:137956.

doi: 10.1016/j.matlet.2024.137956

45. Chaugule PS, Du W, Kamath RR, Barua B, Messner MC, Singh D. Reliability comparisons between additively manufactured and conventional SiC-Si ceramic composites. *J Am Ceramic Soc*. 2024;107(5):3117-3133.

doi: 10.1111/jace.19682

46. Yu YT, Naik GK, Lim YB, Yoon JM. Sintering behavior of spark plasma sintered SiC with Si-SiC composite nanoparticles prepared by thermal DC plasma process. *Nanoscale Res Lett*. 2017;12(1):606.

doi: 10.1186/s11671-017-2370-8

47. Zhang ZH, Wang FC, Luo J, Lee SK, Wang L. Processing and characterization of fine-grained monolithic SiC ceramic synthesized by spark plasma sintering. *Mater Sci Eng A*. 2010;527(7-8):2099-2103.

doi: 10.1016/j.msea.2009.12.027